MAX-PLANCK-INSTITUT FÜR PLASMAPHYSIK

GARCHING BEI MÜNCHEN

Discretization Errors at Free Boundaries of the Grad-Schlüter-Shafranov Equation

Rita Meyer-Spasche and Bengt Fornberg

IPP 6/295 October 1990

Die nachstehende Arbeit wurde im Rahmen des Vertrages zwischen dem Max-Planck-Institut für Plasmaphysik und der Europäischen Atomgemeinschaft über die Zusammenarbeit auf dem Gebiete der Plasmaphysik durchgeführt.

Discretization errors at free boundaries of the Grad-Schlüter-Shafranov equation

Rita Meyer-Spasche [1]

Bengt Fornberg [2]

To Professor LOTHAR COLLATZ on his 80th birthday

Summary The numerical error of standard finite-difference schemes is analyzed at free boundaries of the Grad-Schlüter-Shafranov equation of plasma physics. A simple correction strategy is devised to eliminate (to leading order) the errors which arise as the free boundary crosses the rectangular grid at irregular locations. The resulting scheme can be solved by Gauss-Newton or Inverse iterations, or by multigrid iterations. Extrapolation (from 2^{nd} to 3^{rd} order of accuracy) is possible for the new scheme.

Subject classifications: AMS(MOS): 65N10, 65N05, 35J60. CR: G1.8

short running title: Discretization errors at free boundaries

---

[1] Max-Planck-Institut für Plasmaphysik, IPP–EURATOM Association, *D* 8046 Garching, FRG, FAX (089) 3299-2200

[2] Exxon Research & Engineering Co., Annandale, NJ 08801, USA.

Summary of contents:

1. INTRODUCTION

In magnetohydrodynamic equilibrium computations, the location of the plasma – vacuum interface is not known in advance. It is a free surface, to be determined while solving the equations. Several ways of doing this have been employed. In some of the codes equations for the forces at the interface are added. A convenient approach for axisymmetric equilibria is to "ignore" the free boundary when defining the grid. This strategy was used both with finite difference schemes and with finite elements (see, for example, [7, 11, 4, 9, 15, 5]).

The discretization error of this approach is investigated in Section 2. For 2nd order centered differences ($O(h^2)$ convergence on problems without free boundary), the residual is $O(h)$ in a neighborhood of the free boundary. But this neighborhood is of order h. Thus $O(h^2)$ convergence is obtained globally, with less favorable constants than in the regular cases. The size of the maximum error depends on the position of the grid points with respect to the free boundary. Higher order methods reduce to $O(h^2)$ methods unless there is special treatment of the free boundary. Extrapolation $h \to 0$ is of doubtful value. As a consequence, a naive application of multigrid methods might fail to converge in h. This is demonstrated in Fig. 2.6 of Section 2.4.

A modification of the standard 2D difference scheme is devised in Section 3 such that the residual becomes $O(h^2)$ locally. The global error is reduced and becomes independent of the location of the grid points with respect to the free boundary.

1.1 THE MODEL EQUATIONS

An axisymmetric plasma equilibrium can be modeled by the Grad-Schlüter- Shafranov equation (see, for instance, [2, Chap. 4], [12], or [16]):

$$\Delta^* \psi + I\, I' + R^2\, p' = 0, \tag{1.1.1}$$

$$\Delta^* = \frac{\partial^2}{\partial R^2} - \frac{1}{R}\frac{\partial}{\partial R} + \frac{\partial^2}{\partial z^2},$$

for the flux function ψ in a plasma region Ω_p. Here, R , ϕ and z are cylindrical coordinates, $p(\psi)$ is the pressure, $B_\phi = I(\psi)/R$ is the toroidal magnetic field, and primes indicate differentiation with respect to ψ. The poloidal field $\vec{B}_p$ is related to ψ by

$$\vec{B}_p = \nabla\phi \times \nabla\psi. \tag{1.1.2}$$

We consider the case where a plasma is contained in a conducting shell, but separated from it by a vacuum region Ω_v. With this shell coinciding with a magnetic surface, ψ becomes constant there:

$$\psi = \alpha < 0 \quad \text{on} \quad \partial\Omega = \partial(\bar{\Omega}_p \cup \Omega_v). \tag{1.1.3}$$

We suppose further that there are no singularities (wires) in the vacuum region Ω_v. Then we have

$$\Delta^*\psi + I\ I' + R^2\ p' = 0 \quad \text{in} \quad \Omega_p \tag{1.1.4}$$

and

$$\Delta^*\psi = 0 \quad \text{in} \quad \Omega_v.$$

Since the magnetic field is continuous on the plasma surface, ψ and $\frac{\partial\psi}{\partial n}$ are continuous across $\partial\Omega_p$. The total toroidal plasma current J is usually prescribed as a normalization (cf. [11]):

$$J = -\int_{\Omega_p} \frac{1}{R}\Delta^*\psi\ dR\ dz = -\oint_{\partial\Omega_p} \vec{B}\ d\vec{l} = -\oint_{\partial\Omega} \vec{B}\ d\vec{l} = -\oint_{\partial\Omega} \frac{1}{R}\frac{\partial\psi}{\partial n}\ dl \tag{1.1.5}$$

Temam [16] considered the following model problems:

General assumptions: Let $\Omega \subset R^2$ be a domain bounded with respect to the x_1 - coordinate ($x_* < x_1 < x^*$) and having a smooth boundary ($\partial\Omega \in C^4$). Let $\mathcal{L}$ be a uniformly elliptic operator in Ω,

$$\mathcal{L}\ u := \sum_{i=1}^{2} \frac{\partial}{\partial x_i}\left(\frac{1}{x_1}\frac{\partial u}{\partial x_i}\right) = \frac{1}{x_1}\Delta^*\ u, \tag{1.1.6}$$

and let $b \in C^1(\Omega)$ satisfy $0 < b_1 \leq b(x) \leq b_2$ in $\bar{\Omega}$.

Problem A: Given Ω and a constant $I \neq 0$, find u, λ, γ, and Ω_p with $\bar{\Omega}_p \subset \Omega$, $u(x) \neq 0$ in Ω_p, such that

$$\mathcal{L}\ u = \begin{cases} -\lambda b u & \text{in} \quad \Omega_p \\ 0 & \text{in} \quad \Omega_v := \Omega \backslash \bar{\Omega}_p \end{cases}$$

$$u|_{\partial\Omega} = \gamma,\ \gamma \text{ unknown}, \quad u|_{\partial\Omega_p} = 0, \frac{\partial u}{\partial n} \text{ continuous across } \partial\Omega_p \text{ , and} \tag{1.1.7}$$

$$-\oint_{\partial\Omega_p} \frac{1}{x_1} \frac{\partial u}{\partial n}\, ds = I.$$

Remark 1: Once a solution to this problem is found, we see that λ is the eigenvalue of the subproblem

$$\mathcal{L}\ u + \lambda\ b\ u = 0 \quad \text{in} \quad \Omega_p, \qquad u|_{\partial\Omega_p} = 0. \tag{1.1.8}$$

Owing to the character of elliptic problems, it is in general not possible to find a solution to the full problem from an eigenfunction on some given subdomain $\Omega_p \subset \Omega$.

Remark 2: Problem A is homogeneous. Thus we can multiply any solution by constants to obtain other solutions with the same λ and Ω_p. The integral side condition

$$-\oint_{\partial\Omega_p} \frac{1}{x_1} \frac{\partial u}{\partial n} ds = I \tag{1.1.9}$$

thus plays the role of a normalization.

Remark 3: The condition $\bar{\Omega}_p \subset \Omega$ (excluding the case of the free boundary touching the fixed boundary $\partial\Omega$) makes sense as a plasma close to a wall would destroy it. Mathematically, this condition has been considered to be convenient. It allows solutions to be renormalized by replacing the conditions

$$-\oint_{\partial\Omega_p} \frac{1}{x_1} \frac{\partial u}{\partial n} ds = I, \tag{1.1.10}$$

$$u|_{\partial\Omega} = \gamma, \qquad \gamma \text{ unknown},$$

by the simpler and more standard condition

$$u|_{\partial\Omega} = -1, \tag{1.1.11}$$

thus leading to

Problem B: Let $\Omega \subset R^2$ be given. Find u, λ, Ω_p with $\bar{\Omega}_p \subset \Omega$, $u(x) \neq 0$ in Ω_p, such that

$$\mathcal{L}\ u = \begin{cases} -\lambda b u \text{ in } & \Omega_p \\ 0 \text{ in } & \Omega_v := \Omega \backslash \bar{\Omega}_p \end{cases}$$

$$u|_{\partial\Omega_p} = 0, \quad u|_{\partial\Omega} = -1, \quad \frac{\partial u}{\partial n} \text{ continuous across } \partial\Omega_p.$$

The mapping between the solutions of Problem A and Problem B, however, creates a singularity (see Section 2.1). We thus find it more convenient to reformulate Problem A to include the limiting case $\partial\Omega \equiv \partial\Omega_p$ (see Sections 1.2 and 1.3). Among the results obtained by Temam [16] it is found that the solutions to Problems A and B exist and

i. are holomorphic in Ω_p and in $\Omega_v = \Omega \backslash \Omega_p$,

ii. have Hölder-continuous second derivatives in $\bar{\Omega}$ (i.e. the solutions are $C^{2+\alpha}(\bar{\Omega})$, $0 \leq \alpha < 1$),

iii. their 3^{rd} derivatives are in L^p, $p \geq 1$ (i.e. the solutions are in $W^{3,p}$, $p \geq 1$).

1.2 EXAMPLE

We consider the free-boundary problem

$$\begin{aligned} \psi'' + \lambda^2 \psi^+ &= 0 \qquad \text{in } (0,1), \\ \psi(0) = \psi(1) &= \alpha, \\ \psi'(0) - \psi'(1) &= I, \end{aligned} \tag{1.2.1}$$

where $\psi^+(x) = \begin{cases} \psi(x) & \text{if } \psi(x) > 0 \\ 0 & \text{if } \psi(x) \leq 0 \end{cases}$. Assuming symmetry of the solution, we make the ansatz

$$\psi(x) = \begin{cases} a + b\,x & \text{if} \quad 0 \leq x \leq x_f \\ c\ \sin\lambda(x - x_f) & \text{if} \quad x_f \leq x \leq 1 - x_f \\ a + b(1 - x) & \text{if} \quad 1 - x_f \leq x \leq 1 \end{cases}. \tag{1.2.2}$$

The continuity of ψ and ψ' in the free-boundary point x_f, the fact that λ^2 is the eigenvalue

of $\frac{\partial^2}{\partial x^2}$ in the interval $(x_f, 1-x_f)$, and the boundary conditions provide five equations for the six unknowns λ, α, x_f, a, b, and c. Therefore, we can choose one of these parameters. Prescribing the inner parameter x_f gives good insights and explains why there exist no solutions for certain values of α, $I = 2b$, λ , and $\psi_{\max} = c$. We find

$$0 \le x_f = -\frac{\alpha}{b} < \frac{1}{2} \quad \Rightarrow \quad \pi \le \lambda = \frac{\pi}{1-2x_f} < \infty \quad \text{and} \quad 0 \le c = \frac{b}{\lambda} \le \frac{b}{\pi}. \tag{1.2.3}$$

Fig. 1.1 and Fig. 2.2 show solutions to eq. (1.2.1).

1.3 NUMERICAL MODEL.

We now return to equations (1.1.4), (1.1.5). Let $R_{\min}$ and $R_{\max}$ be the extremum values of the radius R in Ω. We non-dimensionalize and introduce coordinates x and y by

$$\epsilon := \frac{R_{\max} - R_{\min}}{R_{\min}}, \qquad R = R_{\min}(1 + \epsilon\, x), \qquad z = (R_{\max} - R_{\min})\, y, \tag{1.3.1}$$

$$I = R_{\min}\tilde{I}, \quad p = \tilde{p}, \qquad \psi = R_{\min}^2\, \epsilon\, \tilde{\psi}$$

and get (after dropping the tildes and other minor changes)

$$\frac{\partial^2\psi}{\partial x^2} - \frac{\epsilon}{1+\epsilon x}\frac{\partial\psi}{\partial x} + \frac{\partial^2\psi}{\partial y^2} = -\lambda\, \psi^+(1 - \beta_p + \beta_p(1+\epsilon x)^2) \tag{1.3.2}$$

in $D := (0,1) \times (b_1, b_2)$. Here, ϵ measures the curvature of the torus, $\epsilon = 0$ corresponding to planar geometry (straight cylinder). Also, we introduced β_p to vary the degree to which the poloidal currents contribute to the confinement. Our way of non-dimensionalizing slightly differs from that employed by Lortz [12]. The other equations become

$$-\oint_{\partial D} \frac{1}{1+\epsilon x}\frac{\partial\psi}{\partial n}\, dl = J, \tag{1.3.3a}$$

$$(1-\tau)\psi + \tau\frac{\partial\psi}{\partial n} = (1-\tau)g \quad \text{on} \quad \partial D, \tag{1.3.3b}$$

where

$$\psi^+ := \begin{cases} \psi & \text{if } \psi(x,y) > 0 \\ 0 & \text{if } \psi(x,y) \le 0 \end{cases},$$

$g(x,y)$ is an arbitrary function,

$\tau(x,y)$ is a function satisfying $\tau(0,y) = \tau(1,y) = 0$, $b_1 \leq y \leq b_2$ and

$\tau(x,b_i) = c_i, \quad i = 1,2, \quad 0 \leq c_1,\ c_2 \leq 1$.

Equation (1.3.3b) is closely related to "Schaeffer's boundary conditions" [3, 14]. Equations (1.3.2), (1.3.3) contain both Problem A and Problem B as special cases. But they are more convenient in the following respects:

i. The plane case is obtainable from the toroidal case in a smooth limit (see [12]).

ii. The 1D case is a special case. Also, it is possible to impose symmetry with respect to the R-axis.

iii. General boundary conditions allow us to compute solutions to Problem A in non-rectangular domains.

iv. The free boundary is allowed to coincide with the fixed boundary.

The computational domain D is sketched in Fig. 1.2.

1.4 IMPLEMENTATION

First we discretize equations (1.3.2), (1.3.3) by conventional second-order finite differences (local errors $O(h^2)$ on 'regular' problems). The location of the free boundary is ignored in this approach (employed by, for example, Lackner [11], Johnson et al [9], Blum [4] and Braams [5] in their codes for computing 2D plasma equilibria). The resulting nonlinear system of equations is then solved with Gauss-Newton iterations (details below).

1.4.1 Discretization of L_ϵ. The elliptic operator L_ϵ in (1.3.2) can be discretized by

standard central finite differences in two main ways:

$$\psi_{xx} - \frac{\epsilon}{1+\epsilon x}\psi_x + \psi_{yy} \doteq \frac{1}{h^2}\begin{bmatrix} & 1/k^2 & \\ 1+\frac{h}{2}\frac{\epsilon}{1+\epsilon x} & -2-\frac{2}{k^2} & 1-\frac{h}{2}\frac{\epsilon}{1+\epsilon x} \\ & 1/k^2 & \end{bmatrix}\psi \qquad (1.4.1.1)$$

(where $h = h_x$, $k = \frac{h_y}{h_x}$) and

$$(1+\epsilon x)\left(\frac{\psi_x}{1+\epsilon x}\right)_x + \psi_{yy} \doteq$$

$$\frac{1}{h^2}\begin{bmatrix} & 1/k^2 & \\ \frac{1+\epsilon x}{1+\epsilon(x-h/2)} & -\frac{1+\epsilon x}{1+\epsilon(x+h/2)} - \frac{1+\epsilon x}{1+\epsilon(x-h/2)} - \frac{2}{k^2} & \frac{1+\epsilon x}{1+\epsilon(x+h/2)} \\ & 1/k^2 & \end{bmatrix}\psi. \qquad (1.4.1.2)$$

Although numerical experiments seemed to show slightly smaller errors for (1.4.1.2) than for (1.4.1.1), the differences were not significant.

1.4.2. Normal derivatives at the boundary. The integral in (1.3.3) is approximated by the trapezoidal rule and $\frac{\partial\psi}{\partial n}$ by the one-sided $O(h^2)$-accurate, unsymmetric 3-point formula, which reads in case of the lower boundary

$$-\frac{\partial\psi}{\partial y}(x_i, b_1) \doteq -\frac{1}{2h_y}(-3\ \psi_{i,N2} + 4\ \psi_{i,N2-1} - \psi_{i,N2-2}). \qquad (1.4.2.1)$$

Instead of discretizing the condition $\frac{\partial\psi}{\partial y} = 0$ in (1.3.3b), we assume the solution to be symmetric across $x \equiv b_i$, $i = 1, 2$, introduce mirror points outside the domain and use the governing equation at the grid points with $x \equiv b_i$. This satisfies $\frac{\partial\psi}{\partial n} \to 0$ for $h \to 0$ and introduces new non-zero elements only within the band.

1.4.3. Newton's method. We solve the discretized analog of equations

$$L_\epsilon\ \psi + Q(\psi, \lambda; \epsilon) = 0 \quad \text{in} \quad D,$$

$$(1-\tau)\psi + \tau\frac{\partial\psi}{\partial n} = (1-\tau)g \quad \text{on} \quad \partial D, \qquad (1.4.3.1)$$

$$-\oint_{\partial D} \frac{1}{1+\epsilon x}\frac{\partial \psi}{\partial n}dl - I =: T_\epsilon(\psi,\lambda,I) = 0$$

by Newton's method:

$$\begin{pmatrix} L+Q_\psi^n & Q_\lambda^n \\ T_\psi^n & T_\lambda^n \end{pmatrix} \begin{pmatrix} \psi^{n+1}-\psi^n \\ \lambda^{n+1}-\lambda^n \end{pmatrix} = -\begin{pmatrix} L\,\psi^n + Q^n \\ T^n \end{pmatrix}. \tag{1.4.3.2}$$

Here, subscripts denote partial derivatives, superscripts the iteration number and Q_ψ^n the Jacobian matrix $\frac{\partial Q}{\partial \psi}(\psi^n,\lambda^n)$. In the case of $Q(\psi,\lambda) = \lambda\psi^+(1-\beta_p+\beta_p(1+\epsilon x)^2)$, a diagonal element of the Jacobian makes a jump

$$\lambda(1-\beta_p+\beta_p(1+\epsilon x)^2) \tag{1.4.3.3}$$

each time the boundary passes a grid point. For small grid spacings, this is small compared with the element itself (of size $-\frac{2}{h_x{}^2} - \frac{2}{h_y{}^2}$) and appears to cause no difficulties.

The discrete analog of (1.4.3.2) is solved by a (pivoted) Gaussian band-solver applied to $(L+Q_\psi^n)_h$ together with a 'bordering algorithm' (as described by Keller [10]). It involves the steps

$$\begin{aligned} (L+Q_\psi^n)y^{n+1} &= Q_\lambda^n, \\ (L+Q_\psi^n)z^{n+1} &= -L\,\psi^n - Q^n, \\ q^{n+1} = \lambda^{n+1}-\lambda^n &= (-T_\psi^n z^{n+1} - T^n)/(T_\lambda^n - T_\psi^n y^{n+1}), \\ p^{n+1} = \psi^{n+1}-\psi^n &= z^{n+1} - y^{n+1}q^{n+1} \end{aligned} \tag{1.4.3.4}$$

with the boundary conditions

$$\begin{aligned} (1-\tau)y^{n+1} + \tau\frac{\partial y^{n+1}}{\partial n} &= 0, \\ (1-\tau)z^{n+1} + \tau\frac{\partial z^{n+1}}{\partial n} &= 0, \end{aligned} \tag{1.4.3.5}$$

ensuring that

$$(1-\tau)p^{n+1} + \tau\frac{\partial p^{n+1}}{\partial n} = 0 \tag{1.4.3.6}$$

and thus

$$(1-\tau)\psi^{n+1} + \tau\frac{\partial\psi^{n+1}}{\partial n} = (1-\tau)g \tag{1.4.3.7}$$

if ψ^0 satisfies this boundary condition.

1.5 EXPLICITLY KNOWN SOLUTIONS

Several solutions to eqs (1.3.2), (1.3.3) can be given explicitly:

1.5.1 Example 1 (1D, $\epsilon = 0$). As already discussed in Section 1.2, the differential equation

$$\begin{aligned} &\psi'' + \lambda^2\psi^+ = 0 \quad \text{in} \quad (0,1), \\ &\psi(0) = \psi(1) = \alpha, \\ &\psi'(0) - \psi'(1) = I \end{aligned} \tag{1.5.1.1}$$

is solved by

$$\psi(x) = \begin{cases} a + I\ x & \text{if} \quad 0 \le x \le x_f \\ c\ \sin\lambda(x - x_f) & \text{if} \quad x_f \le x \le 1 - x_f \\ a + I(1-x) & \text{if} \quad 1 - x_f \le x \le 1 \end{cases} \tag{1.5.1.2}$$

with free boundary in

$$x_f := -\frac{\alpha}{I} \in (0, \frac{1}{2}) \tag{1.5.1.3}$$

and eigenvalue

$$\lambda = \frac{\pi}{1 - 2x_f}. \tag{1.5.1.4}$$

1.5.2 Example 2 (2D, $\epsilon = 0$). Equation

$$\Delta\psi + \lambda^2\psi^+ = 0 \tag{1.5.2.1}$$

in a circle can be reduced to the ODE

$$\psi'' + \frac{1}{r}\psi' + \lambda^2 \psi^+ = 0. \tag{1.5.2.2}$$

If we pick a solution with free boundary at radius r_f, we get

$$\psi(r) = \begin{cases} J_0(\lambda\, r) & \text{if} \quad 0 \le r \le r_f \\ A \ln \frac{r}{r_f} & \text{if} \quad r \ge r_f \end{cases} \tag{1.5.2.3}$$

with

$$\lambda\, r_f = j_{0,1} \quad \text{(first zero of } J_0) \tag{1.5.2.4}$$

and

$$A = \lambda\, r_f\, J_0'(\lambda\, r_f) = j_{0,1}\, J_0'(j_{0,1}) \tag{1.5.2.5}$$

$$\oint_{r=r_f} \frac{\partial \psi}{\partial n}\, dl = 2\, \pi A. \tag{1.5.2.6}$$

This solution has already been given by Bandle [1].

In our numerical experiments, we chose the origin $r = 0$ to be situated in the center $(1/2, 1/2)$ of the unit square $D = (0,1) \times (0,1)$, and prescribed the function values of the exact solution on ∂D. Solutions to (1.5.2.2) with

$$\oint_{\partial D} \frac{\partial \psi}{\partial n}\, dl = 2\, \pi A \tag{1.5.2.7}$$

and $r_f = 0.2$ and $r_f = 0.4$ are displayed in Fig. 2.3. The curvature (2nd derivatives) strongly increases for $r_f \to 0$. As a consequence, the discretization errors also increase if the grid is kept fixed and r_f is diminished. The limiting case of the solution is a cusp.

1.5.3 Example 3 (1D, $\epsilon \neq 0, \beta_p = 1$). Equation

$$w'' - \frac{1}{r} w' + \lambda^2\, r^2\, w^+ = 0, \tag{1.5.3.1}$$

$$w(r_1) = w(r_4) = \alpha$$

is solved by

$$w(r) = \begin{cases} a_1 + \frac{b_1}{2}\, r^2 & \text{if} \quad r_1 \le r \le r_2 \\ c\, \sin \frac{\lambda}{2}(r^2 - r_2^2) & \text{if} \quad r_2 \le r \le r_3 \\ a_3 + \frac{b_3}{2} r^2 & \text{if} \quad r_3 \le r \le r_4 \end{cases} \tag{1.5.3.2}$$

with $r_1 > 0$, $r_4 = 1 + r_1$, $\alpha < 0$, $b_3 < 0$ and

$$a_3 = \alpha - \frac{b_3}{2} r_4^2, \quad b_1 = -b_3, \quad a_1 = \alpha + \frac{b_3}{2} r_1^2,$$

$$r_2^2 = -2\,\frac{a_1}{b_1}, \quad r_3^2 = -2\,\frac{a_3}{b_3}, \quad \lambda = \frac{2\pi}{r_3^2 - r_2^2}, \quad c = -\frac{b_3}{\lambda}, \tag{1.5.3.3}$$

provided that

$$2\alpha + \frac{b_3}{2}(r_1^2 - r_4^2) = -\frac{b_3}{2}(r_3^2 - r_2^2) > 0. \tag{1.5.3.4}$$

With $\epsilon = 1/r_1$, $r = r_1(1 + \epsilon x)$ and $\psi(x) = \epsilon\, w(r_1(1 + \epsilon x))$ we get solutions of

$$\psi'' - \frac{\epsilon}{1 + \epsilon x}\psi' + \lambda^2 (1 + \epsilon x)^2 \psi^+ = 0, \tag{1.5.3.5}$$

$$\psi(0) = \psi(1) = \alpha.$$

A solution of (1.5.3.5) is shown in Fig. 3.3. The parameter values are given there.

1.5.4 Example 4 (1D, $\epsilon \neq 0, \beta_p = 0$). Equation

$$w'' - \frac{1}{r} w' + \lambda^2\, w^+ = 0 \tag{1.5.4.1}$$

is solved by

$$w(r) = \begin{cases} a_1 + \frac{b_1}{2}\, r^2 & \text{if} \quad r_1 \le r \le r_2 \\ c\, r\, J_1(\lambda\, r) & \text{if} \quad r_2 \le r \le r_3 \\ a_3 + \frac{b_3}{2} r^2 & \text{if} \quad r_3 \le r \le r_4 \end{cases} \tag{1.5.4.2}$$

with

$$\lambda > 0, \quad \lambda\, r_2 = j_{1,1}, \quad \lambda\, r_3 = j_{1,2}, \quad \gamma := \frac{J_1'(j_{1,2})}{J_1'(j_{1,1})},$$

$$r_1 = \frac{\gamma}{\gamma + 1}\left(-1 + \sqrt{1 + \frac{r_2^2 + \gamma r_3^2 - \gamma}{\gamma^2}(1 + \gamma)}\right), \quad r_4 = 1 + r_1, \tag{1.5.4.3}$$

provided that

$$r_1^2 - r_2^2\, \gamma (r_4^2 - r_3^2) = 0.$$

Here $j_{1,1}$ and $j_{1,2}$ are the first two zeroes of the Bessel function J_1. With $\epsilon := 1/r_1$, $r = r_1(1+\epsilon x)$ and $\psi(x) = \epsilon\, w(r_1(1+\epsilon x))$ we get solutions of

$$\psi'' - \frac{\epsilon}{1+\epsilon x}\psi' + \lambda^2\psi^+ = 0, \qquad (1.5.4.4)$$
$$\psi(0) = \psi(1) = \alpha$$

by computing the remaining parameters of eq. (1.5.4.2) in the obvious way. A solution of (1.5.4.4) is shown in Fig. 1.3.

2. THE DISCRETIZATION ERRORS

2.1 PREVIOUS RESULTS

Lackner [11] solved the nonlinear MHD equilibrium problem by inverse iteration, combined with a fast Poisson solver for the linear equations. He investigated the accuracy of his computations in the presence of a free boundary by solving a problem with discontinuous right-hand side both numerically with his code and by evaluating a Green's function expression. Since the conductor causing the discontinuity was always placed on a grid point, $\max\|\text{error}\| = C \cdot h^2$ was obtained when $^1/_{32} \le h \le {}^1/_{256}$, provided the computations with $h \le {}^1/_{64}$ were performed in IBM "double precision" (i.e. about 16 decimal places of accuracy) (unpublished).

Rappaz [13] and Caloz & Rappaz [6] give theoretical error estimates for Galerkin / finite-element methods. In [13], Rappaz considers

$$\Delta u + \lambda\, u^+ = 0 \qquad \text{in } \Omega, \qquad (2.1.1)$$
$$u = -1 \qquad \text{on } \partial\Omega.$$

He uses the auxiliary problem

$$\Delta v + \lambda\, v^+ = 0 \qquad \text{in } \Omega, \qquad (2.1.2)$$
$$v = -\epsilon \qquad \text{on } \partial\Omega,$$
$$(v, \varphi) = 1 - (\epsilon, \varphi),$$

to parametrize the solution set of (2.1.1) by the mapping

$$(\lambda(\epsilon), u(\epsilon)) := (\lambda(\epsilon), \frac{1}{\epsilon}\, v(\epsilon)). \tag{2.1.3}$$

Here, $\epsilon \in (-\bar{\epsilon}\ ,\ \bar{\epsilon})$ is the parameter, φ the normalized eigenfunction of Ω (i.e. the solution of (2.1.2) for $\epsilon = 0$), and (v, φ) the L^2 scalar product. The bottom relation in (2.1.2) implies the condition

$$(u, \varphi) = \frac{1}{\epsilon} - (1, \varphi) \tag{2.1.4}$$

for the solutions u of (2.1.1) and produces a 'bifurcation from infinity' for $\epsilon = 0$. With piecewise linear elements and triangularizations with diameters $\leq h$ in a polygonial domain Ω, he obtains the error estimates

$$\begin{aligned} |\lambda(\epsilon) - \lambda_h(\epsilon)| &\leq C\ h \\ \|u(\epsilon) - u_h(\epsilon)\|_{1,\Omega} &\leq C\ h\ \epsilon^{-1} \end{aligned} \tag{2.1.5}$$

for $0 < \epsilon \leq \bar{\epsilon}$, C being a constant independent of h and ϵ. The relative errors

$$\frac{\|u(\epsilon) - u_h(\epsilon)\|_{1,\Omega}}{\|u(\epsilon)\|_{1,\Omega}} \leq \bar{C}h \text{ for } 0 < \epsilon \leq \bar{\epsilon} \tag{2.1.6}$$

are independent of ϵ, since $\|\epsilon\ u(\epsilon) - \varphi\| = \|v(\epsilon) - \varphi\| \to 0 \quad$ for $\epsilon \to 0$.

Using similar techniques, Caloz & Rappaz [6] prove $O(h)$-convergence for piecewise quadratic finite elements applied to the more general problem

$$\begin{aligned} -\Delta u &= \lambda\{u^+ + \mu(u^+)^2\} \quad \text{in } \Omega, \\ u &= -\epsilon \qquad \text{on } \partial\Omega, \\ -\oint_{\partial\Omega} \frac{\partial u}{\partial n}\, ds &= I, \end{aligned} \tag{2.1.7}$$

where $I > 0$ is fixed and (ϵ, μ) lies in a neighborhood of $(0, 0)$.

2.2 SOME TEST CASES

In order to investigate the discretization error of our numerical approach in the presence of a free boundary, we performed the following experiments:

i. Take an explicitly known solution (λ, ψ) from Section 1.5, with

$$T(\psi, \lambda, 0) = \int_{\partial D} \frac{1}{1+\epsilon x} \frac{\partial \psi}{\partial n}\, ds =: J \tag{2.2.1}$$

ii. Use Gauss-Newton iterations to compute a numerical solution (λ_h, ψ_h) with

$$T_h(\psi_h, \lambda_h, 0) = J$$

as side condition, as described in Section 1.4.

iii. Stop the iteration process when

$$\|L_h \psi_h^n + Q_h^n\|_\infty < 5 \cdot 10^{-8} \qquad \text{and} \qquad |\lambda_h^{n+1} - \lambda_h^n| < 5 \cdot 10^{-8}, \tag{2.2.2}$$

(see (1.4.3.4); Owing to rounding errors, $5 \cdot 10^{-8}$ is the maximum accuracy obtainable in some of the examples).

iv. Compute the errors

$$\frac{|\psi(x,y) - \psi_h(x,y)|}{\psi(\frac{1}{2}, \frac{1}{2})}, \qquad \frac{|\lambda - \lambda_h|}{\lambda}, \qquad \frac{|J - T_h(\psi_h, \lambda_h, 0)|}{J}. \tag{2.2.3}$$

As a first example, we show in Fig. 2.1 the errors obtained for the solution of

$$\begin{aligned} \Delta\psi + \lambda\, \psi &= 0 \qquad \text{in } D := (0,1) \times (0,1), \\ (1-\tau)\psi + \tau \frac{\partial \psi}{\partial n} &= 0 \qquad \text{on } \partial D, \\ \tau(x,y) &= \begin{cases} 0 & \text{if } x = 0 \text{ or } x = 1 \\ 1 & \text{if } y = 0 \text{ or } y = 1 \end{cases} \\ -\oint_{\partial D} \frac{\partial \psi}{\partial n}\, ds &= 2, \end{aligned} \tag{2.2.4}$$

as computed with $h_x = {}^1/_8, {}^1/_{16}, \ldots, {}^1/_{512}$ and $h_y = {}^1/_2$. Theoretically, this is equivalent to

$$\begin{aligned} \psi'' + \lambda\, \psi &= 0, \\ \psi(0) = \psi(1) &= 0, \\ \psi'(0) - \psi'(1) &= 2. \end{aligned} \tag{2.2.5}$$

Rounding errors are more important in (2.2.4) than in (2.2.5). The main difference, however, is due to the change in normalization: the numerical error in (2.2.4) is dominated by the truncation error of (1.4.2.1). Since

$$y_0'' - \frac{y_{-1} - 2\,y_0 + y_1}{h^2} \approx \frac{h^2}{3\cdot 4}\; y_0^{IV} = \frac{h^2\pi^4}{3\cdot 4}\; y_0, \tag{2.2.6}$$

the truncation error of (1.4.1.1) is proportional to the exact function value in every grid point: If there is no numerical error in the computation of the norm of the solution, we get (up to rounding errors) the exact function values.

Consider how the errors of the trapezoidal rule compare with the errors in computing $\frac{\partial\psi}{\partial n}$ by means of (1.4.2.1):

$$\frac{\partial\psi_0}{\partial n} - \frac{1}{2h}(-3\;\psi_0 + 4\;\psi_1 - \psi_2) \approx \frac{1}{3}h^2\psi'''(0) = -h^2\frac{\pi^2}{3} \approx -h^2\cdot 3.289868, \tag{2.2.7}$$

The values obtained for the last quantity in (2.2.3) are, after division by h^2,

1/h	8	16	32	64	128	256	512
C	3.1152	3.2457	3.2788	3.2871	3.2892	3.2897	3.2898

(2.2.8)

Although the error estimates (2.2.6), (2.2.7) are valid only for $h \to 0$, we see in Fig. 2.1 that the asymptotic constants are almost reached already for $h = {}^1/_{16}$. The deviation is 5.3 % for $h = {}^1/_8$ and $2\cdot 10^{-3}$% for $h = {}^1/_{512}$.

A completely different picture is obtained for

$$\begin{aligned} &\psi'' + \lambda\;\psi^+ = 0, \\ &\psi(0) = \psi(1) = -\frac{1}{5}, \\ &\oint_{\partial D}\frac{\partial\psi}{\partial n}\,ds = 2. \end{aligned} \tag{2.2.9}$$

Fig. 2.2a shows that, in this case, the error is *bounded* by Const$\cdot h^2$, but only the errors in the global quantity λ are *equal to* $C\cdot h^2$ for some constant C. (Since the solution is linear outside the free boundary, the numerical approximation of (2.2.9) is there accurate to the rounding error level.) An analysis of the position of the free boundary with respect to the

grid points for the different values of h suggests that the error depends on the distance between the free boundary and the nearest grid point. This is confirmed by Fig. 2.2b, which shows cases where h was chosen such that the free boundary always becomes located at a grid point.

Looking at Fig. 2.3, Example 2,

$$\begin{aligned} \Delta\psi + \lambda\ \psi^{+} &= 0 \qquad \text{in } D := (0,1)\times(0,1), \\ \psi|_{\partial D} &= g, \\ \oint_{\partial D} \frac{\partial\psi}{\partial n}\, ds &= J, \end{aligned} \tag{2.2.10}$$

(where g and J attain the values of the exact solution), we see that $errors/h^2$ (with $h = h_x = h_y$) behave quite smoothly when the plasma range is large ($r_f = 0.4$ or $x_f = 0.1$), but they are larger and behave more similarly to what is shown in Fig. 2.2a for smaller plasma regions ($r_f = 0.2$ or $x_f = 0.3$).

2.3 ANALYSIS OF THE TEST CASES

To understand the experimentally observed behavior, we approximate the 1D solutions, around the free boundary, by 3^{rd}-order polynomials. We consider first the case when the vacuum region is to the left, and the free boundary is located between the center and farthest right point of the (3-point) difference stencil (cf. Fig. 2.4a). λ is kept fixed at its exact value. To third order, the function values of the analytic solution at the grid points are

$$\begin{aligned} \psi(-h) &= -\beta(h+z), \\ \psi(0) &= -\beta\ z, \\ \psi(h) &= \beta(h-z) - \frac{\beta\ \lambda(h-z)^3}{6}, \end{aligned} \tag{2.3.1}$$

where z is the grid point to free boundary distance and β is the value of ψ_x at the interface. With these expressions, we compute the residual as

$$R_1 = \frac{1}{h^2}[1 \quad -2 \quad 1]\psi$$

$$= \frac{1}{h^2}\{\{-\beta(h+z)\} - 2\{-\beta z\} + \{\beta(h-z)\} - \frac{\beta\lambda(h-z)^3}{6}\}\} \qquad (2.3.2)$$
$$= \frac{\beta\lambda}{6h^2}(z-h)^3.$$

This expression is visualized in Fig. 2.4b. The case $-h \leq z \leq 0$ is treated in the same way. With $\psi(0) = -\beta z + \frac{\beta\lambda}{6}z^3 > 0$ (including the ψ^+ term), we get

$$\begin{aligned} R_2 &= \frac{1}{h^2}[1 \quad -2 \quad 1]\psi + \lambda[0 \quad 1 \quad 0]\psi \\ &= \frac{\beta\lambda}{3h^2}\{-z^3 - \frac{1}{2}(h-z)^3\} + \beta\lambda\{-z + \frac{\lambda}{6}z^3\} \qquad (2.3.3) \\ &= -\frac{\beta\lambda}{6h^2}(z+h)^3 + \frac{\beta\lambda^2}{6}z^3. \end{aligned}$$

To leading order, this remainder (shown in Fig. 2.4d) is the mirror image of the previous case.

To sum up: Let the solution ψ of

$$\begin{aligned} \psi'' + \lambda\ \psi^+ &= 0, \\ \psi(0) = \psi(1) &= \alpha, \qquad (2.3.4) \\ \psi'(0) &= \beta \end{aligned}$$

be locally approximated by cubics and let the difference scheme suddenly change at $z \in [-h, h]$:

$$\frac{1}{h^2}[1 \quad -2 \quad 1]\psi + \lambda[0 \quad 1 \quad 0]\psi^+ = 0, \qquad (2.3.5)$$

then:

i. The residual is

$$d(z) = \begin{cases} 0 \\ \frac{\beta\lambda}{6h^2}(|z|-h)^3 \end{cases} + O(h^3) \text{ for } \begin{cases} |z| \geq h \\ |z| < h \end{cases} . \qquad (2.3.6)$$

ii. Max $|d(z)|$ occurs for $z = 0$, *i.e.* when the free boundary is located at a grid point.

iii. If the free boundary is located half-way between two grid points, two stencils will be affected, but each cubic is down to $^1/_8{}^{th}$ of its maximum value. Therefore, the total

error is down to $^1/_4{}^{th}$ of the 'at a grid point' case. This is confirmed by two series of computations (with the choice of $\alpha = -^1/_4$ in (2.3.4)). In the case of $\{h = {}^1/_8\ ,\ {}^1/_{16}\ ,\ \ldots\ ,\ {}^1/_{512}\}$, the interface at $x_f = {}^1/_4$ is always located at a grid point, whereas in the case $\{h = {}^1/_{10}\ ,\ {}^1/_{18}\ ,\ {}^1/_{34}\ ,\ {}^1/_{66}\ ,\ {}^1/_{130}\ ,\ {}^1/_{258}\ ,\ {}^1/_{514}\}$ it always falls half-way in-between two grid points. Results are shown in Fig. 2.5.

2.4 FURTHER TEST CASES: Multigrid Computations

As we have seen in the previous sections, the actual error depends on the distance free boundary – grid points. This typically varies when a grid is refined (only in 1D, $\epsilon = 0$, could we keep it constant). This observation led us to expect that there are convergence problems in h for multigrid computations.

In Fig. 2.6 we show three sets of computations with program MG00D of [8] and a slightly changed main program for equations

$$\begin{aligned} -\Delta_h \psi_h &= \lambda_{ex}\ \psi^+_{ex} \qquad \text{in } D := (0,1) \times (0,1), \\ \psi_h|_{\partial D} &= \psi_{ex}|_{\partial D}. \end{aligned} \tag{2.4.1}$$

Here the subscript 'h' denotes quantities affected by discretization, while the subscript 'ex' means that we use values of the explicit solution of Example 2. The deviation from eq. (2.2.10) is necessary because MG00D solves

$$\begin{aligned} -\Delta \psi &= f \qquad \text{in } D := (0,1) \times (0,1), \\ \psi|_{\partial D} &= g \end{aligned} \tag{2.4.2}$$

with known functions f and g which have to be given as Fortran FUNCTIONs.

In the first set of computations, we treated a case without free boundary : $r_f = 0.8$, see Fig. 2.6c. Here multigrid shows its full power. Convergence is $O(h^2)$, and storage requirements are minimal. Much finer discretizations are possible than for the computations of Fig. 2.3.

In the next set of computations, we chose $r_f = 0.6$. In this case the free boundary cuts the fixed boundary, as shown in Fig. 2.6c. Convergence is $O(h^2)$ down to $h = {}^1/_{32}$, and then the error stagnates. Further refinement of the grid does not bring any improvement.

In the last set of computations, we chose $r_f = 0.4$. This is the case of Fig. 2.3a. In this case, the minimal obtainable error is already obtained for $h = {}^1/_8$.

Properties of MG00D:

Difference operators: usual 5-point stars on all grids;

coarsening: h, 2h, 4h, ...;

relaxation: red - black;

fine to coarse: half-injection; coarse to fine: bilinear interpolation;

full multigrid interpolation uses grid equation (4th order).

The quantity m in the abscissa of Fig. 2.6a and Fig. 2.6b gives $\log_2 h$ for the finest grid used in each computation. The routine contains several parameters that allow one to vary the cycling (V, W, number of relaxations, ...). A change of these parameters did not make any difference.

3. A CORRECTION STRATEGY

3.1 THE SIMPLEST CASE (1D, $\epsilon = 0$)

3.1.1 The scheme. Now that we know the $O(h)$ portion of the residual (equations (2.3.2) and (2.3.3)), we can compensate for it by changing the difference scheme locally. Let the differential equation

$$\psi'' + \lambda\, \psi^+ = 0 \qquad (3.1.1.1)$$

be given and the interval be partitioned by grid points x_j with spacing h. Let the free boundary be situated between x_{i_1} and x_{i_1+1} , as sketched in Fig. 2.4a (vacuum region to the left of this boundary), and again between x_{i_2} and x_{i_2+1}. Then we use the following

scheme:

$$\begin{array}{llll}
\frac{1}{h^2}[1-2 \quad 1]\psi & & = 0, & j < i_1 \\
\frac{1}{h^2}[1-2 \quad 1]\psi & + \frac{\lambda}{6}\frac{\psi_{i_1+1}^3}{(\psi_{i_1+1}-\psi_{i_1})^2} & = 0, & j = i_1 \\
\frac{1}{h^2}[1-2 \quad 1]\psi + \lambda \quad \psi_{i_1+1} & - \frac{\lambda}{6}\frac{\psi_{i_1}^3}{(\psi_{i_1+1}-\psi_{i_1})^2} & = 0, & j = i_1+1 \\
\frac{1}{h^2}[1-2 \quad 1]\psi + \lambda \quad \psi_j & & = 0, & i_1+1 < j < i_2,
\end{array} \tag{3.1.1.2}$$

and similarly for the second interface. Fig. 3.1 shows computations with this scheme for $x_f = {}^1/_5$. We see that the errors in the function values now converge in higher than 2^{nd} order, while the error in λ has not changed (cf. Fig. 2.2).

3.1.2. Derivation of the new scheme. Let us consider Fig. 2.4a again. Since

$$\begin{aligned}
\psi(h) &= \beta(h-z) - \frac{\beta\lambda}{6}(h-z)^3 \qquad (3.1.2.1)\\
\psi(0) &= -\beta z,
\end{aligned}$$

we get

$$\begin{aligned}
\beta &= \frac{\psi(h)-\psi(0)}{h} + \frac{\beta\lambda}{6}(1-\frac{z}{h})^3 h^2 \qquad (3.1.2.2)\\
z &= -\frac{\psi(0)}{\beta}.
\end{aligned}$$

Using (3.1.2.2) in (2.3.2) gives

$$R_1 = -\frac{\beta\lambda}{6h^2}(h-z)^3 = -\frac{\lambda}{6}\frac{\psi(h)^3}{(\psi(h)-\psi(0))^2} + O(h^3). \tag{3.1.2.3}$$

Similarly, we get for $-h \le z \le 0$

$$R_2 = \frac{\lambda}{6}\frac{\psi(-h)^3}{(\psi(0)-\psi(-h))^2} + O(h^3). \tag{3.1.2.4}$$

With a consistent numbering of the grid points, this gives the scheme (3.1.1.2).

3.1.3 Implementation of the new scheme. To implement the new scheme, we have to find the appropriate indices i_1, i_2 (where the discrete function ψ changes sign), and then alter the discrete analog of Q (cf. eq. (1.4.3.1)) by the four quantities $R_1(i_1)$, $R_2(i_1+1)$,

$R_2(i_2)$, and $R_1(i_2+1)$. While the derivatives of Q only affect the diagonal of the Jacobian, the derivatives of $Q+R$ involve off-diagonal elements as well. The modifications caused by the new scheme alter 8 off-diagonal entries, which all fall within the previous band structure.

During the testing phase, we implemented scheme (3.1.1.2) stepwise:

i. We treated the position of the free boundary as given, and changed only the residual in the second equation of (1.4.3.4), thus saving the work of computing derivatives. This reduced the discretization error in the function values to $O(h^4)$, see Fig. 3.2. For large h, $h \geq {}^1/_{32}$, convergence of this partial Newton method was considerably slowed down in comparison with the original scheme. For small h , $h \leq {}^1/_{128}$, convergence of these iterations was not affected.

ii. We treated the position of the free boundary as unknown (*i.e.* searched for the indices i_1, i_2), but still used only partial Newton. There was poor convergence in some of the cases $h \geq {}^1/_{16}$, but no convergence problems for $h \leq {}^1/_{32}$.

iii. We implemented the full scheme (3.1.1.2). The derivatives are approximated by their discrete analogs, according to

$$\frac{\partial R_i}{\partial \psi_j}(\psi_j, \psi_k) \doteq \frac{R_i(\psi_j + d, \psi_k) - R_i(\psi_j, \psi_k)}{d}. \qquad (3.1.3.1)$$

As variations in d between $10^{-2} \cdot h_x$ and $10^{-5} \cdot h_x$ were found to have no influence on the convergence rate, we routinely used $d = 10^{-2} \cdot h_x$.

Comparisons between partial and full implementations (Fig. 3.2) show only very small differences; in both cases we got $O(h^4)$ for the function values and $O(h^2)$ for the eigenvalue. Because of ii. we think that it will be possible (and advantageous) to use the generalization of scheme (3.1.1.2) with Lackner's inverse iteration [11], and also with multigrid.

3.2 THE GENERAL 1D CASE ($\epsilon \neq 0$)

For the more general equation

$$\psi'' - \frac{\epsilon}{1+\epsilon x}\psi' = -\lambda\ \psi^+(1-\beta_p+\beta_p(1+\epsilon x)^2), \tag{3.2.1}$$

a local analysis in a neighborhood of the free boundary shows that the immediate generalization of (3.1.1.4),

$$\begin{array}{llllll}
\frac{1}{h^2}[1 \quad -2 \quad 1]\psi & -\frac{b_j}{2h}[-1 \quad 0 \quad 1]\psi & & & = 0 & j < i, \\
\frac{1}{h^2}[1 \quad -2 \quad 1]\psi & -\frac{b_i}{2h}[-1 \quad 0 \quad 1]\psi & & +\frac{\lambda c_i}{6}\frac{\psi_{i+1}^3}{(\psi_{i+1}-\psi_i)^2} & = 0 & j = i, \\
\frac{1}{h^2}[1 \quad -2 \quad 1]\psi & -\frac{b_{i+1}}{2h}[-1 \quad 0 \quad 1]\psi + \lambda c_{i+1}\psi_{i+1} & & -\frac{\lambda c_{i+1}}{6}\frac{\psi_i^3}{(\psi_{i+1}-\psi_i)^2} & = 0 & j = i+1, \\
\frac{1}{h^2}[1 \quad -2 \quad 1]\psi & -\frac{b_j}{2h}[-1 \quad 0 \quad 1]\psi + \lambda\ c_j\psi_j & & & = 0 & i+1 < j,
\end{array} \tag{3.2.2}$$

where

$$b_j := \frac{\epsilon}{1+\epsilon x_j}, \qquad c_j := 1-\beta_p+\beta_p(1+\epsilon x_j)^2, \tag{3.2.3}$$

is indeed the correct generalization. Any first derivative term or any factor in front of ψ^+ can be completely straightforwardly implemented. No special precautions are needed because of the interface. Two sets of computations for Example 3 are shown in Fig. 3.3.

3.3 THE NEW SCHEME IN 2D

3.3.1 Derivation of the scheme. In 1D, corrections were needed whenever the interface occurred on one of the 'legs' of the stencil. In 2D, the similar 'generic situation' is that the interface cuts across either one or two adjacent legs of the 5-point stencil, as illustrated in Fig. 3.4. With slightly altered notation, we number the center grid point 0 and the other four 1, 2, 3 and 4 (counter-clockwise from top). We consider first the situation in Fig. 3.4b and assume ψ_0, ψ_3 , $\psi_4 < 0$, ψ_1, $\psi_2 > 0$. Locally, $\psi(x,y)$ can be considered linear in x and y. This local plane is uniquely determined by the values ψ_0, ψ_1 and ψ_2. Therefore, the interface line (along which $\psi(x,y) = 0$), the distances from this line to the stencil nodes 0, 1 and 2 (denoted d_0, d_1 and d_2, cf. Fig. 3.4c) and the slope this plane forms with the 'horizontal surface' $\psi(x,y) \equiv 0$ (denoted β) can all be expressed in ψ_0, ψ_1 and ψ_2. We assume for simplicity a grid spacing of h in both the x and y directions. Straightforward

geometry leads to the relations

$$d_0^2 = \frac{h^2 {\psi_0}^2}{(\psi_1 - \psi_0)^2 + (\psi_2 - \psi_0)^2},$$
$$d_1^2 = \frac{h^2 {\psi_1}^2}{(\psi_1 - \psi_0)^2 + (\psi_2 - \psi_0)^2}, \qquad (3.3.1.1)$$
$$d_2^2 = \frac{h^2 {\psi_2}^2}{(\psi_1 - \psi_0)^2 + (\psi_2 - \psi_0)^2},$$

and

$$\beta = \frac{\psi_1 - \psi_0}{d_1 + d_0} = \frac{\psi_2 - \psi_0}{d_2 + d_0} = \frac{1}{h}\{(\psi_1 - \psi_0)^2 + (\psi_2 - \psi_0)^2\}^{1/2}.$$

Since the nodes 1 and 2 are located at distances d_1 and d_2 on the other side of the interface (relative to the center node), according to the 1D argument in Section 3.1.2, ψ_1 and ψ_2 have changed by $\frac{\beta\lambda d_1^3}{6}$ and $\frac{\beta\lambda d_2^3}{6}$, respectively, from what they would have been, had the equation not changed at the interface. When applying a stencil like

$$(\frac{1}{h^2}\begin{bmatrix} & 1 & \\ 1 & -4 & 1 \\ & 1 & \end{bmatrix} - \lambda \begin{bmatrix} & 0 & \\ 0 & 1 & 0 \\ & 0 & \end{bmatrix})\psi = 0, \qquad (3.3.1.2)$$

we obtain the corresponding residuals by dividing these changes by h^2. With use of equations (3.3.1.1) we obtain

$$\left[\begin{matrix}\text{Correction } \textit{because} \\ \psi_0 \cdot \psi_1 < 0\end{matrix}\right] = \frac{\lambda}{6} \frac{{\psi_1}^3}{(\psi_1 - \psi_0)^2 + (\psi_2 - \psi_0)^2}$$

and (3.3.1.3)

$$\left[\begin{matrix}\text{Correction } \textit{because} \\ \psi_0 \cdot \psi_2 < 0\end{matrix}\right] = \frac{\lambda}{6} \frac{{\psi_2}^3}{(\psi_1 - \psi_0)^2 + (\psi_2 - \psi_0)^2},$$

resp.

Notes:

i. For each occurrence of an interface cutting across any leg of the 5-point stencil, we simply add (or subtract, depending on the sign of ψ_0), a correction of the form shown in (3.3.1.3).

ii. These 2D corrections immediately reduce to the 1D formulas (3.1.1.2) in case the interface is aligned with the x or y-axis (i.e. $\psi_2 = \psi_0$ and $\psi_1 = \psi_0$, respectively).

iii. As in the 1D case, the presence of first-derivative terms in the governing equations ($\epsilon \neq 0$) will not alter the appropriate correction formulas to leading order in 2D, since their stencils are of the form [function values]$/h$ rather than [function values]$/h^2$.

3.3.2. Implementation and test results. Implementation of this scheme along the lines discussed in Section 3.1.3 gave the expected behavior. Results are displayed in Fig. 3.5 for the test cases of Fig. 2.3. The observations reported in Section 3.1.3 about the 1D case carry over directly. Usage of this new scheme in connection with multigrid should be easy to implement. As a consequence, convergence of the discretization error for $h \rightarrow 0$ can be obtained for multigrid computations in free boundary problems as well.

We believe that our correction strategy will carry over directly to 3D with its 6-leg 7-point stencil for the Laplacian. Until now, we have not carried out the required tests to verify this.

ACKNOWLEDGEMENT

We thank D. Lortz for many discussions and for providing Examples 3 and 4. We thank Chr. Witsch for discussions and for providing a copy of MG00D with main program.

REFERENCES

1. C. Bandle: Abschätzung der Randwerte bei nicht-linearen elliptischen Gleichungen aus der Plasmaphysik. Proc. Oberwolfach, **Numerische Behandlung von Differentialgleichungen, vol.3**, J. Albrecht, L. Collatz, eds. ISNM 56, Birkhäuser Verlag, 1981.
2. G. Bateman: **MHD Instabilities.** The MIT Press, Cambridge, Ma, and London, 1980
3. J.H. Bolstad, H.B. Keller: Computation of anomalous modes in the Taylor experiment. J. Comp Phys **69**, 230 - 251 (1987)
4. J. Blum: **Numerical Simulation and Optimal Control in Plasma Physics**, John Wiley & Sons, 1989
5. B.J. Braams: Computational studies in Tokamak equilibrium and transport, Ph. D. Thesis, U Utrecht, 217 pages, 1986
6. G. Caloz, J. Rappaz: On the numerical approximation of a free boundary problem related to MHD equilibria. Comput. Phys. Comm. **31**, 137 – 141 (1984)

7. W. Feneberg, K. Lackner: Multipole Tokamak equilibria, Nucl. Fusion **13**, 549 (1973)

8. Foerster, Witsch: On efficient multigrid software for elliptic problems on rectangular domains. Math. Comput. Simulation XXIII, 293 – 298 (1981)

9. J.L. Johnson, H.E. Dalhed, J.M. Greene, R.C. Grimm, Y.Y. Hsieh, S.C. Jardin, J. Manickam, M. Okabayashi, R.G. Storer, A.M.M. Todd, D.E. Voss, and K.E. Weimer: Numerical determination of axisymmetric toroidal MHD equilibria. J. Comp Phys **32**, 212 – 234 (1979)

10. H.B. Keller: Numerical solution of bifurcation and nonlinear eigenvalue problems. In: **Applications of Bifurcation Theory**, ed. P. Rabinowitz, Academic Press, 1977, 359 – 384

11. K. Lackner: Computation of ideal MHD equilibria, Comp. Phys. Comm. **12**, 33 – 44 (1976)

12. D. Lortz, On the stability of axisymmetric MHD modes. Z. Naturforsch. **43 a** 1009 – 1016 (1988)

13. J. Rappaz: Approximation of a nondifferentiable nonlinear problem related to MHD equilibria. Numer. Math. **45**, 117 – 133 (1984)

14. D. Schaeffer: Qualitative analysis of a model for boundary effects in the Taylor problem, Math. Proc. Camb. Phil. Soc. **87**, 307 – 337 (1980)

15. M. Sermange: Etude numerique des bifurcations et de la stabilité des solutions des equations de Grad-Shafranov. Proc. **Computing Methods in Applied Sciences and Engineering**, R. Glowinski, J.L. Lions (eds.), North Holland Publishing Company, pp. 93 – 110, 1980

16 R. Temam: A nonlinear eigenvalue problem: the shape at equilibrium of a confined plasma. Arch Rational Mech Anal **60**, 51-73 (1975)

Figure Captions

Fig. 1.1: Sketch of solutions to eq. (1.2.1):
a) typical case $0 < \frac{|\alpha|}{b} < \frac{1}{2}$;
b) limiting case with coinciding fixed and free boundary, $\frac{|\alpha|}{b} = 0$;
c) limiting case in which the inner domain Ω_p is degenerated to the empty set, $\frac{|\alpha|}{b} = \frac{1}{2}$.

Fig. 1.2: Sketch of the computational domain D.

Fig. 1.3: Solution to eq. (1.5.4.4) with $\lambda = 5$, $\alpha = -1$ and $\epsilon \approx 1.85645$.

Fig. 2.1: Numerical error of standard finite differences for the standard 1D eigenvalue problem in 2D formulation, eq. (2.2.4):
a)|rel error|$/h^2$ versus $m := -\log_2 h$. $\sqcup - \sqcap - \sqcup$: relative error in the computation of the integral; $\diamondsuit - \diamondsuit - \diamondsuit$: rel. error in $\psi(\frac{1}{2}, \frac{1}{2})$; $\circ - \circ - \circ$: rel. error in λ;
b) $\log_{10}$ |rel error| versus m; actually, $\log_{10}(|\text{rel error}| + 10^{-17})$ versus m is always plotted since |rel error| = 0 occurred several times.
c) $\psi(x) \cdot 10$ versus x. —— : exact values, $\cdots$: function values, as computed with $h = 1/16$. The error is dominated by the error in $\frac{\partial \psi}{\partial n}$ at the boundary.

Fig. 2.2: Example 1, $x_f = \frac{1}{5}$, $J = 2$.
a) $h = {}^1/_8, {}^1/_{16}, {}^1/_{32}, \ldots, {}^1/_{512}$. x_f is never a grid point, the distance varies;
b) $h = {}^1/_{10}, {}^1/_{20}, {}^1/_{40}, \ldots, {}^1/_{320}, {}^1/_{510}$. x_f is always a grid point.

Fig. 2.3: Example 2, $h_x = h_y = {}^1/_8, {}^1/_{16}, {}^1/_{32}, {}^1/_{64}, {}^1/_{96}$.
a) $r_f = 0.4$, $x_f = 0.1$, $\alpha = \psi(0, \frac{1}{2}) \approx -0.27859$, $\lambda^2 \approx 36.14491$;
b) $r_f = 0.2$, $x_f = 0.3$, $\alpha = \psi(0, \frac{1}{2}) \approx -1.1439$, $\lambda^2 \approx 144.5796$.

Fig. 2.4: a), c): sketch for local analysis of the discretization error in a neighborhood of the free boundary point; z is the distance free boundary - center of stencil;
b), d): the residual as a function of z.

Fig. 2.5: Example 1, $x_f = \frac{1}{4}$, $J = 2$.
a) Computations with $h = 2^{-n}$, $n = 3, \ldots, 9$. The free-boundary points always coincide with grid points.
b) Computations with $h = (2^n + 2)^{-1}$, $n = 3, \ldots, 9$. Each free-boundary point is located in the middle between two grid points. This brings the error in the function values down to $\frac{1}{4}$ of the previous value. (The error in the eigenvalue λ is not affected since λ is a global quantity.)

Fig. 2.6: Example 2. Multigrid computations with routine MG00D of [8] for 3 different

positions of the free boundary:

$r_f = 0.8$, $x_f = -0.3$, (no free boundary in computational domain);

$r_f = 0.6$, $x_f = -0.1$, (free boundary cuts fixed boundary of the computational domain);

$r_f = 0.4$, $x_f = 0.1$, (free boundary fully inside of the computational domain: same case as in Fig. 2.3a).

Fig. 3.1: Example 1, $x_f = \frac{1}{5}$, $J = 2$. Computations with scheme (3.1.1.2) and $h = {}^1/_8, {}^1/_{16}, {}^1/_{32}, \ldots, {}^1/_{512}$. A comparison of this figure with Fig. 2.2a shows that our new scheme considerably smoothens the numerical errors.

Fig. 3.2: Example 1, $x_f = \frac{1}{4}$, $J = 2$. Computations with scheme (3.1.1.2) and $h = {}^1/_8, {}^1/_{16}, {}^1/_{32}, \ldots, {}^1/_{512}$. Comparison of partial implementation of Newton's method (- - -) with full Newton (—). Compare with Fig. 2.5.

Fig. 3.3: Solution to eq. (1.5.3.5), Example 3, with $r_1 = 1$, $\alpha = -0.5$, $b_3 = -1$, and $\epsilon = 1.0$. $x_{f_1} = \sqrt{2} - 1 \approx 0.414$, $x_{f_2} = \sqrt{3} - 1 \approx 0.732$:

a) computations with the standard second order scheme;

b) computations with our new scheme (3.2.2) and full Newton.

Fig. 3.4: Sketch for derivation of eqs. (3.3.1.1) and (3.3.1.3).

Fig. 3.5: Example 2, computed with 2D corrections according to (3.3.1.3), for $h_x = h_y = {}^1/_8, {}^1/_{16}, {}^1/_{32}, {}^1/_{64}, {}^1/_{96}$.

a) $r_f = 0.4$, $x_f = 0.1$, $\alpha = \psi(0, \frac{1}{2}) \approx -0.27859$, $\lambda^2 \approx 36.14491$

b) $r_f = 0.2$, $x_f = 0.3$, $\alpha = \psi(0, \frac{1}{2}) \approx -1.1439$, $\lambda^2 \approx 144.5796$.

See Fig. 2.3 for computations with uncorrected standard scheme.

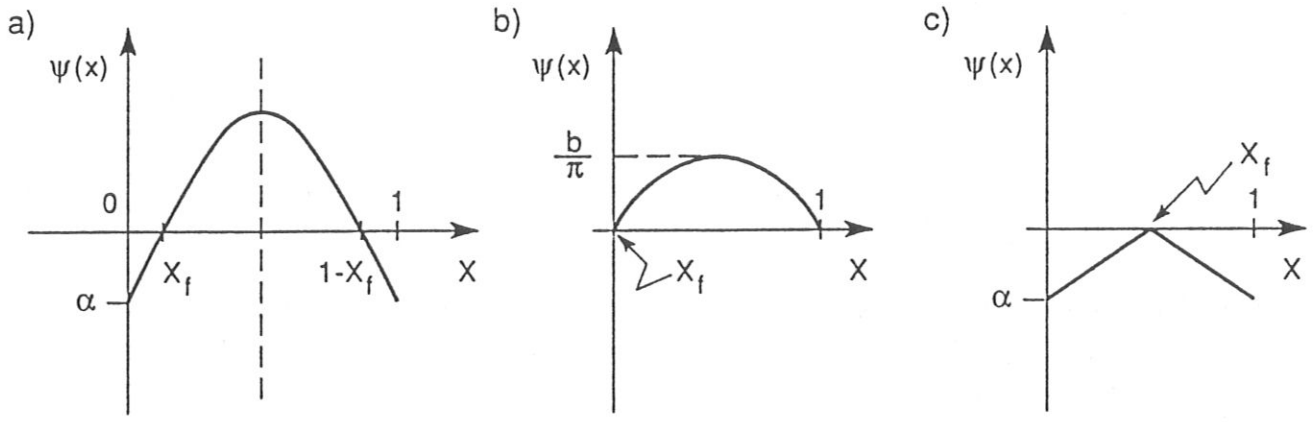

Fig. 1.1: Sketch of solutions to eq. (1.2.1):
a) typical case $0 < \frac{|\alpha|}{b} < \frac{1}{2}$;
b) limiting case with coinciding fixed and free boundary, $\frac{|\alpha|}{b} = 0$;
c) limiting case in which the inner domain Ω_p is degenerated to the empty set, $\frac{|\alpha|}{b} = \frac{1}{2}$.

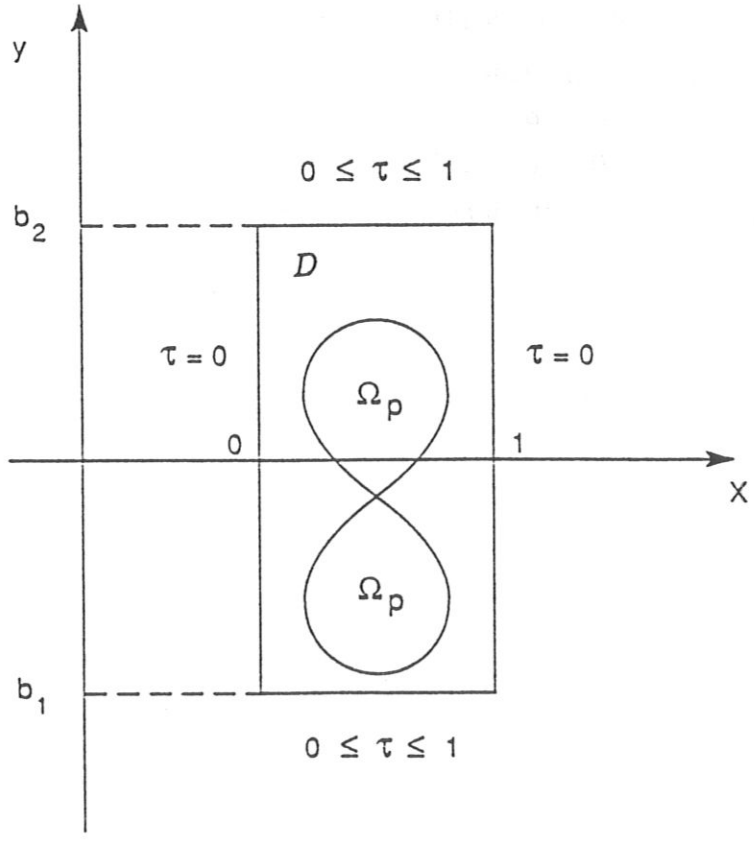

Fig. 1.2: Sketch of the computational domain D.

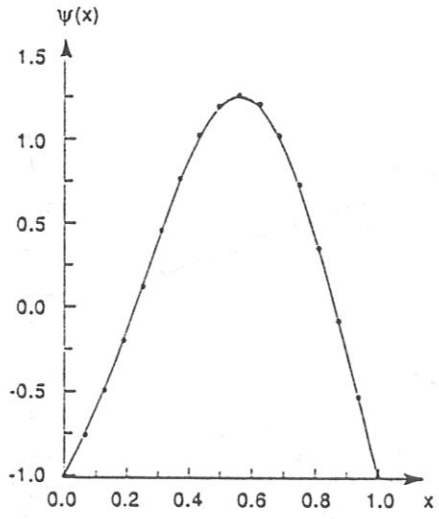

Fig. 1.3: Solution to eq. (1.5.4.4) with $\lambda = 5$, $\alpha = -1$ and $\epsilon \approx 1.85645$.

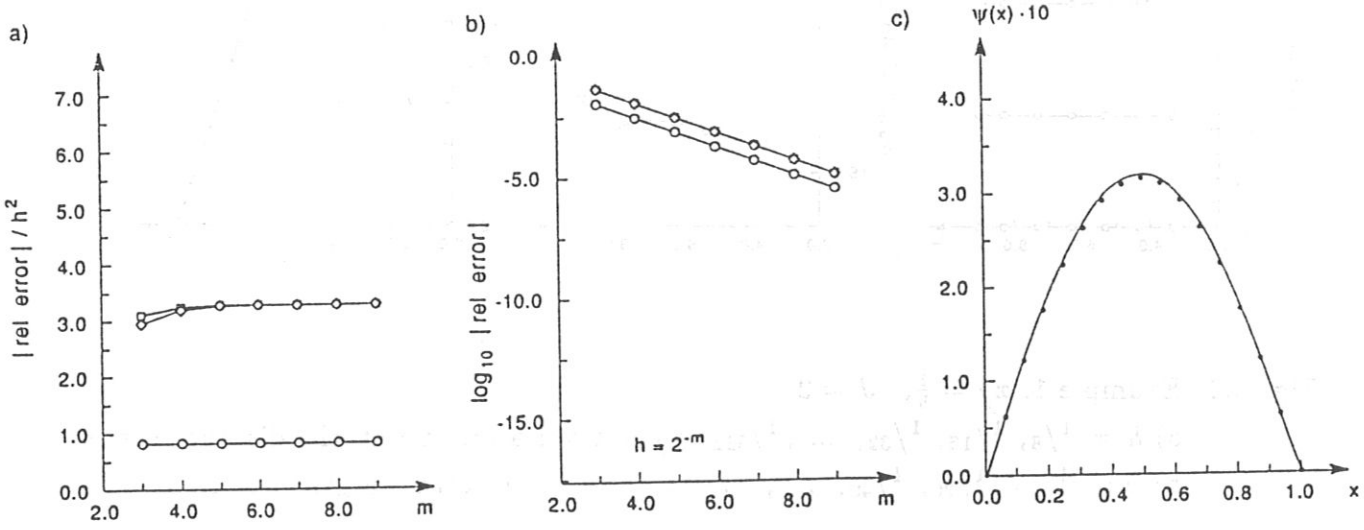

Fig. 2.1: Numerical error of standard finite differences for the standard 1D eigenvalue problem in 2D formulation, eq. (2.2.4):

a)$|\text{rel error}|/h^2$ versus $m := -\log_2 h$. $\square - \square - \square$: relative error in the computation of the integral; $\diamond - \diamond - \diamond$: rel. error in $\psi(\frac{1}{2}, \frac{1}{2})$; $\circ - \circ - \circ$: rel. error in λ;

b) $\log_{10} |\text{rel error}|$ versus m; actually, $\log_{10}(|\text{rel error}| + 10^{-17})$ versus m is always plotted since $|\text{rel error}| = 0$ occurred several times.

c) $\psi(x) \cdot 10$ versus x. —— : exact values, $\cdots$: function values, as computed with $h = 1/16$. The error is dominated by the error in $\frac{\partial \psi}{\partial n}$ at the boundary.

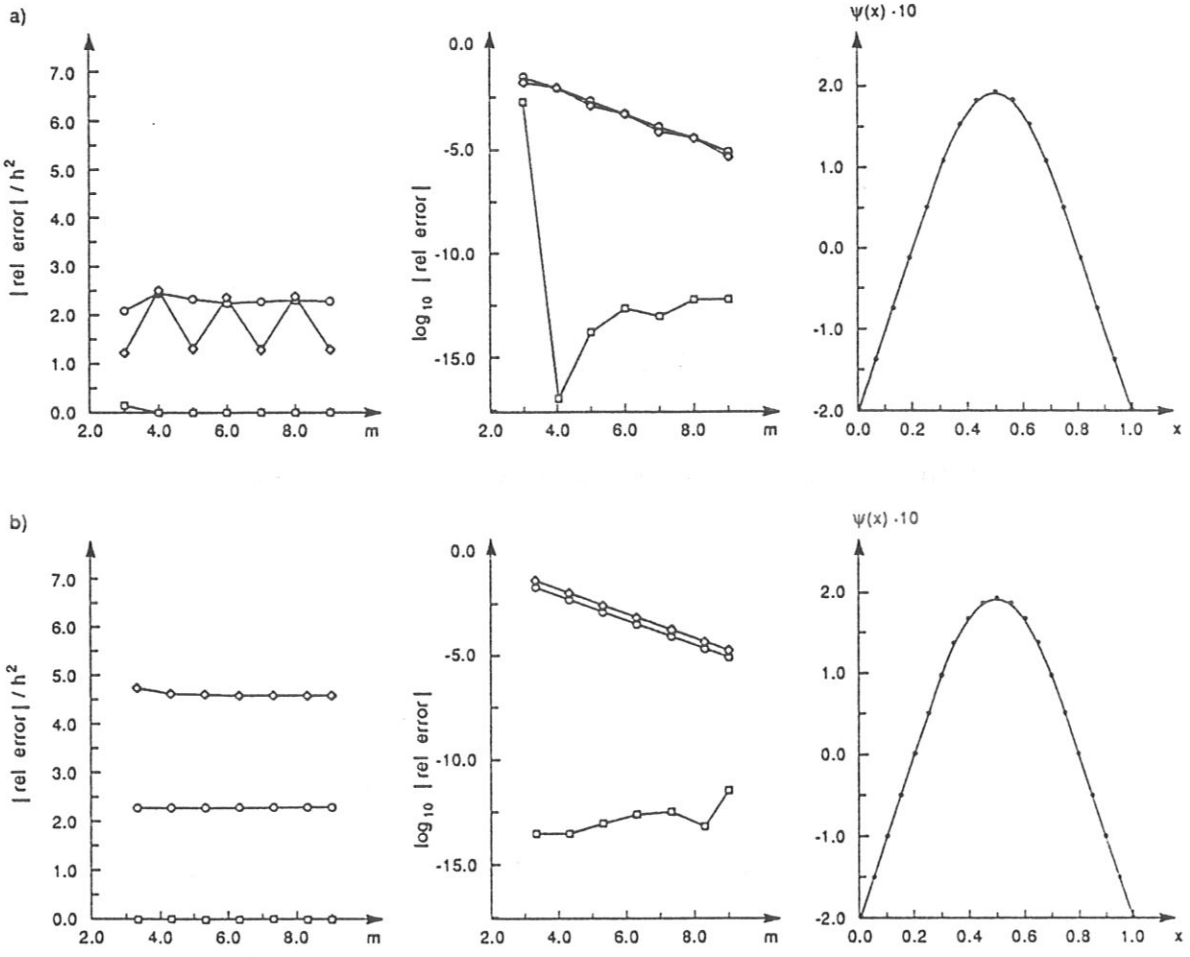

Fig. 2.2: Example 1, $x_f = \frac{1}{5}$, $J = 2$.

a) $h = {}^1/_8,\ {}^1/_{16},\ {}^1/_{32},\ \ldots,\ {}^1/_{512}$. x_f is never a grid point, the distance varies;

b) $h = {}^1/_{10},\ {}^1/_{20},\ {}^1/_{40},\ \ldots,\ {}^1/_{320},\ {}^1/_{510}$. x_f is always a grid point.

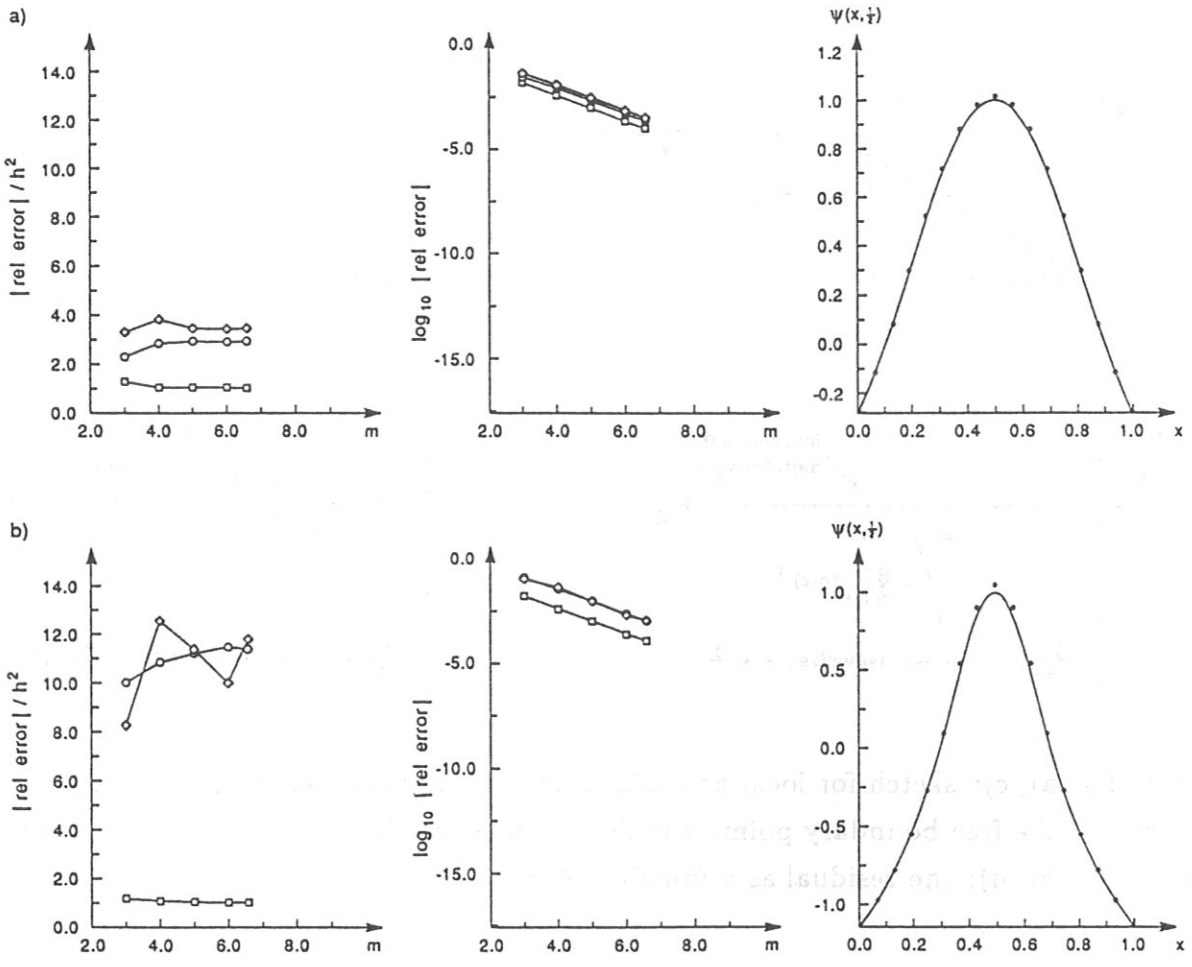

Fig. 2.3: Example 2, $h_x = h_y = {}^1/_8,\ {}^1/_{16},\ {}^1/_{32},\ {}^1/_{64},\ {}^1/_{96}$.
a) $r_f = 0.4,\ x_f = 0.1,\ \alpha = \psi(0, \frac{1}{2}) = -0.27859,\ \lambda^2 = 36.14491$;
b) $r_f = 0.2,\ x_f = 0.3,\ \alpha = \psi(0, \frac{1}{2}) = -1.1439,\ \lambda^2 = 144.5796$.

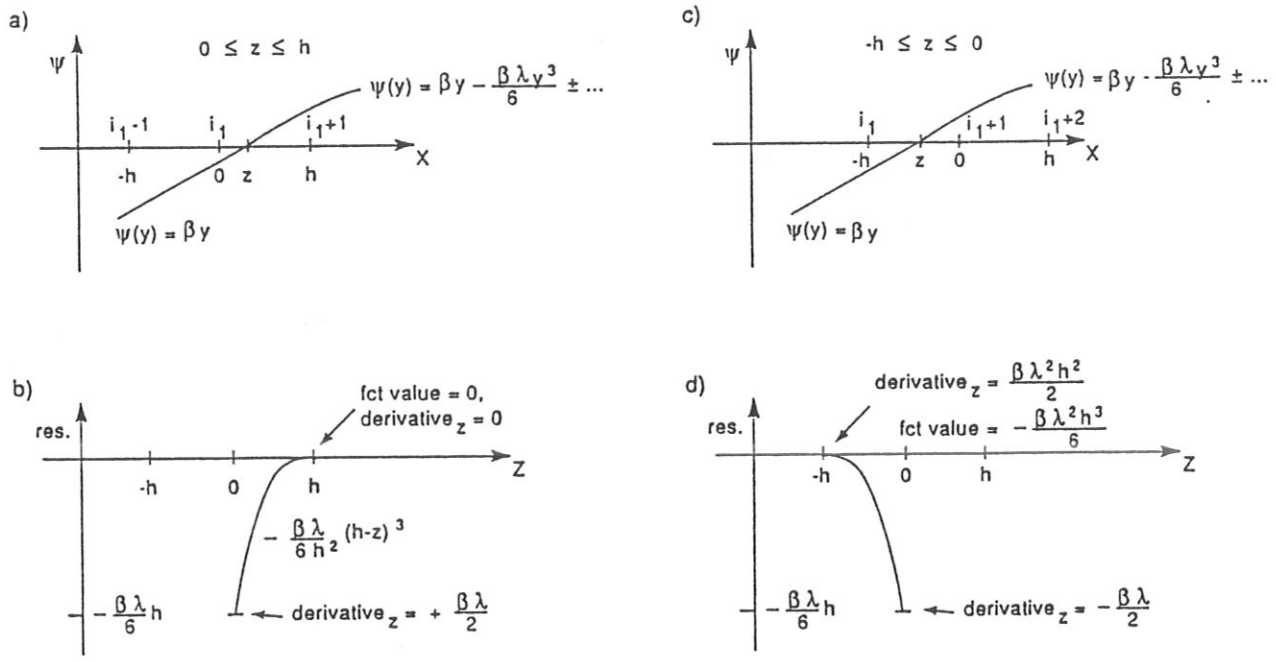

Fig. 2.4: a), c): sketch for local analysis of the discretization error in a neighborhood of the free boundary point; z is the distance free boundary - center of stencil; b), d): the residual as a function of z.

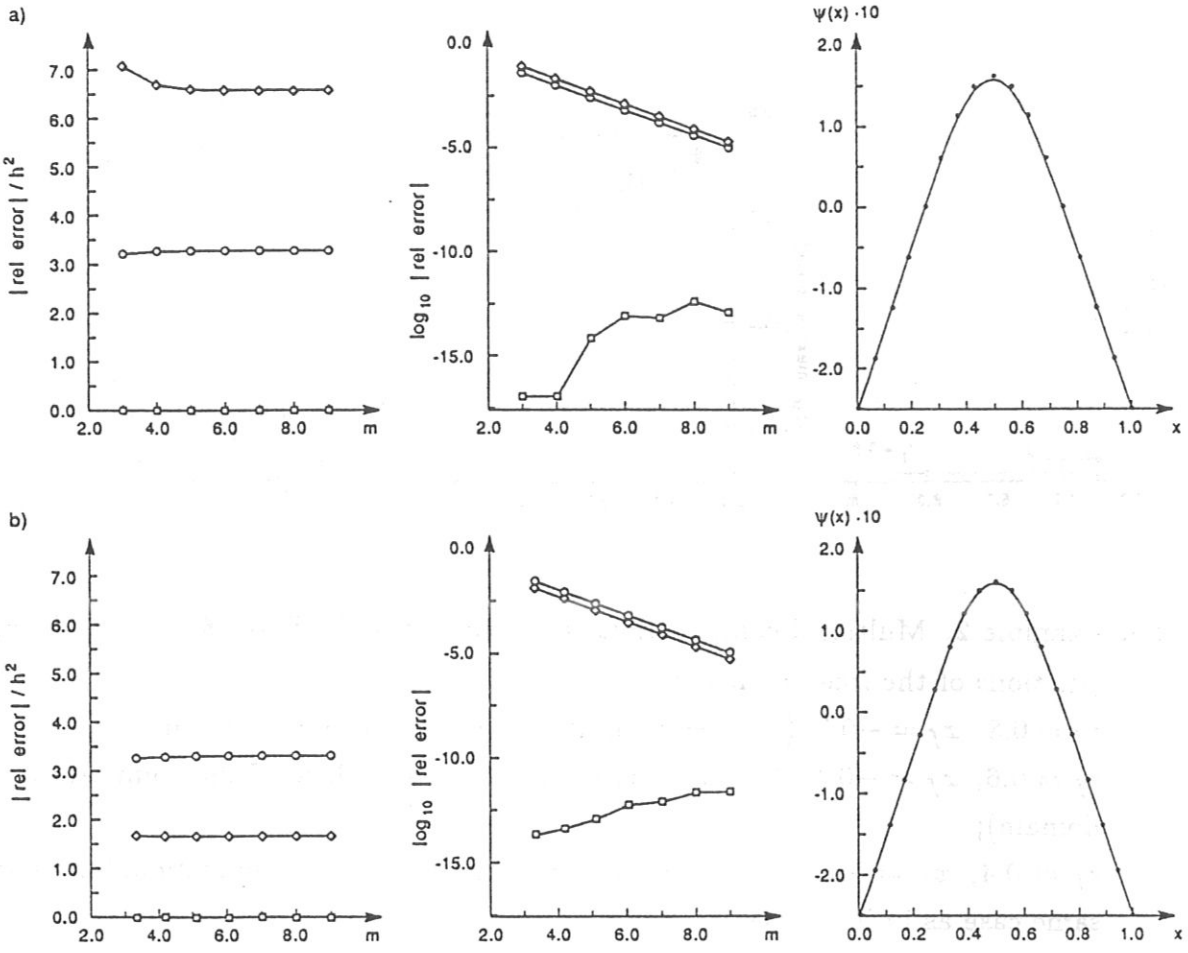

Fig. 2.5: Example 1, $x_f = \frac{1}{4}$, $J = 2$.

a) Computations with $h = 2^{-n}$, $n = 3, ..., 9$. The free-boundary points always coincide with grid points.

b) Computations with $h = (2^n + 2)^{-1}$, $n = 3, ..., 9$. Each free-boundary point is located in the middle between two grid points. This brings the error in the function values down to $\frac{1}{4}$ of the previous value. (The error in the eigenvalue λ is not affected since λ is a global quantity.)

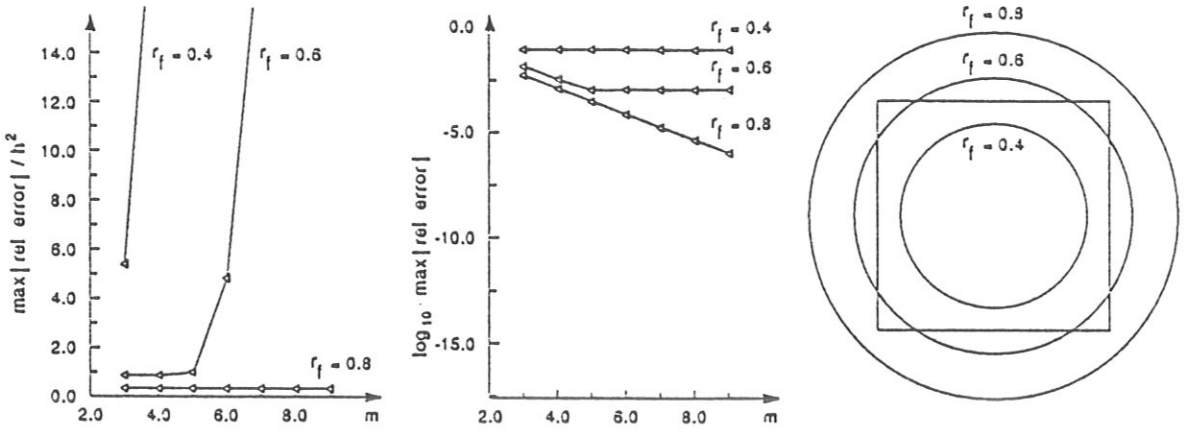

Fig. 2.6: Example 2. Multigrid computations with routine MG00D of [8] for 3 different positions of the free boundary:
$r_f = 0.8$, $x_f = -0.3$, (no free boundary in computational domain);
$r_f = 0.6$, $x_f = -0.1$, (free boundary cuts fixed boundary of the computational domain);
$r_f = 0.4$, $x_f = 0.1$, (free boundary fully inside of the computational domain: same case as in Fig. 2.3a).

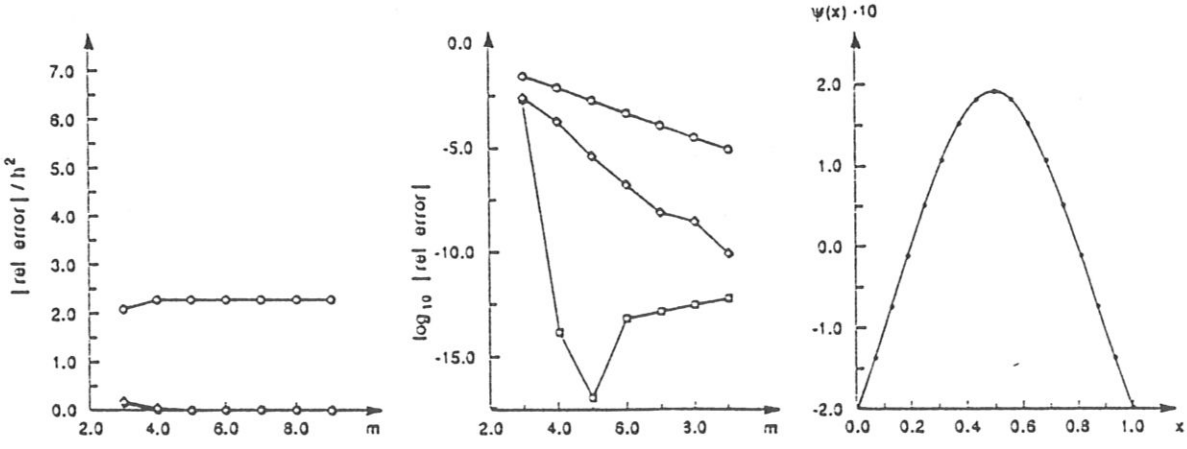

Fig. 3.1: Example 1, $x_f = \frac{1}{5}$, $J = 2$. Computations with scheme (3.1.1.2) and $h = {}^1/_8, {}^1/_{16}, {}^1/_{32}, \ldots, {}^1/_{512}$. A comparison of this figure with Fig. 2.2a shows that our new scheme considerably smoothens the numerical errors.

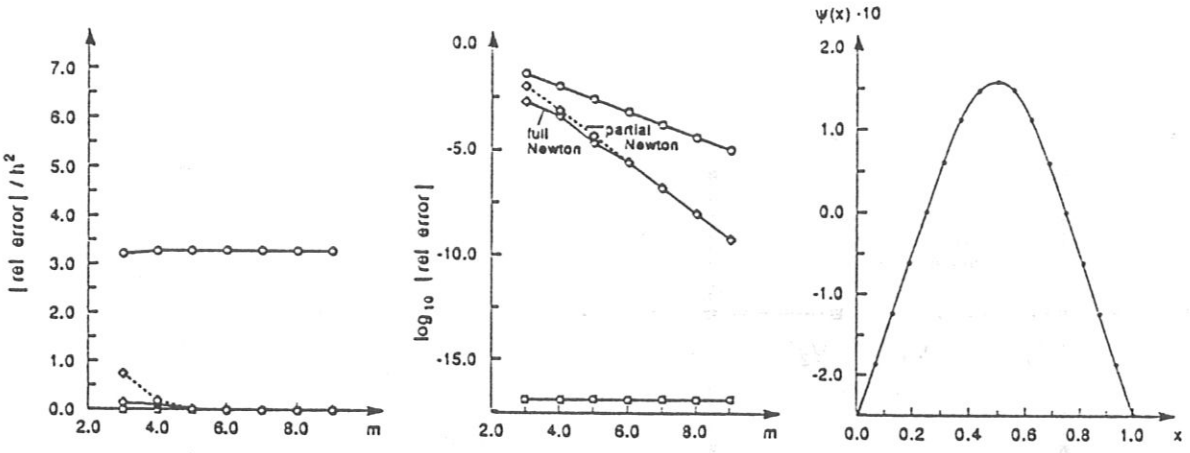

Fig. 3.2: Example 1, $x_f = \frac{1}{4}$, $J = 2$. Computations with scheme (3.1.1.2) and $h = {}^1/_8, {}^1/_{16}, {}^1/_{32}, \ldots, {}^1/_{512}$. Comparison of partial implementation of Newton's method (- - -) with full Newton (—). Compare with Fig. 2.5.

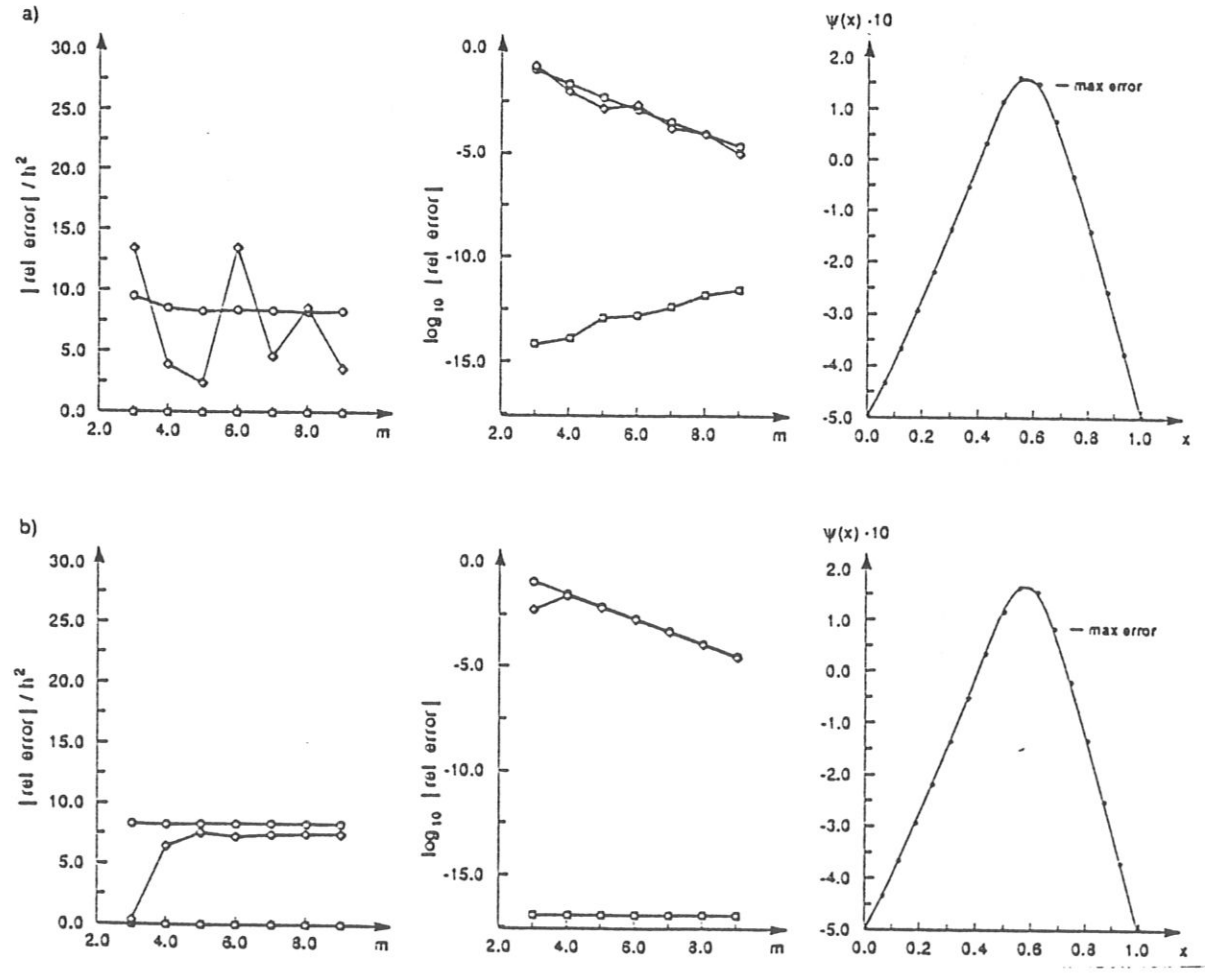

Fig. 3.3: Solution to eq. (1.5.3.5), Example 3, with $r_1 = 1$, $\alpha = -0.5$, $b_3 = -1$, and $\epsilon = 1.0$. $x_{f_1} = \sqrt{2} - 1 \approx 0.414$, $x_{f_2} = \sqrt{3} - 1 \approx 0.732$:

a) computations with the standard second order scheme;

b) computations with our new scheme (3.2.2) and full Newton.

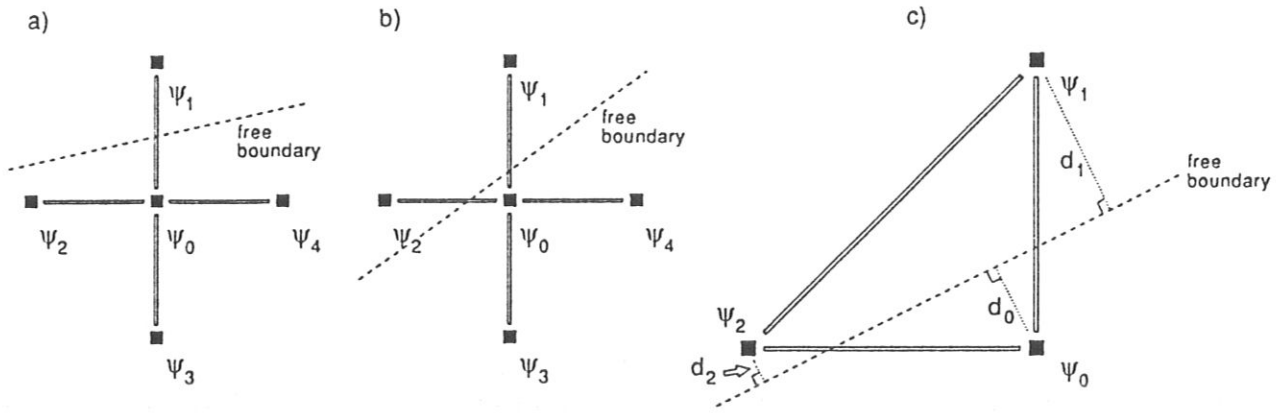

Fig. 3.4: Sketch for derivation of eqs. (3.3.1.1) and (3.3.1.3).

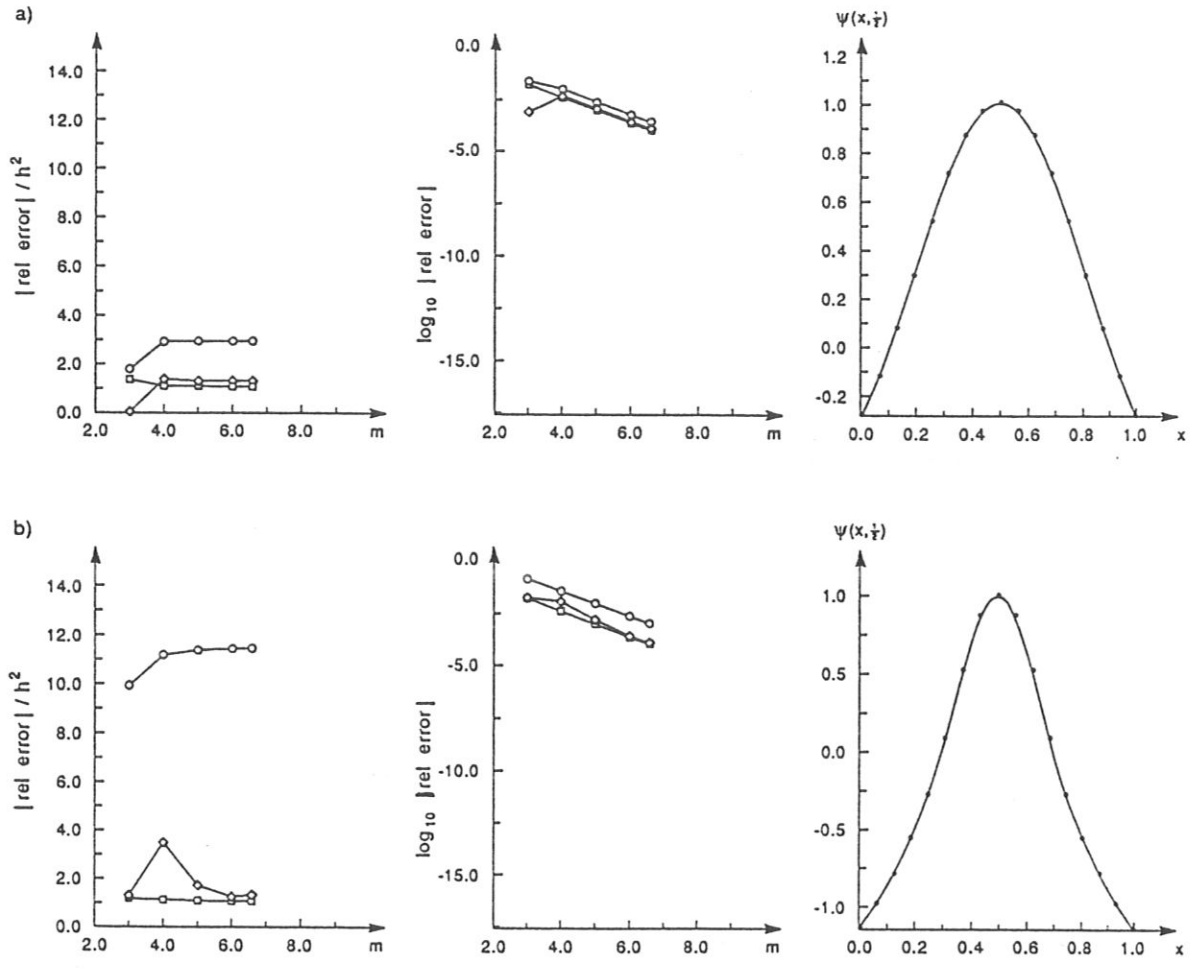

Fig. 3.5: Example 2, computed with 2D corrections according to (3.3.1.3), for $h_x = h_y = {}^1/_8,\ {}^1/_{16},\ {}^1/_{32},\ {}^1/_{64},\ {}^1/_{96}$.

a) $r_f = 0.4,\ x_f = 0.1,\ \alpha = \psi(0, \frac{1}{2}) = -0.27859,\ \lambda^2 = 36.14491$

b) $r_f = 0.2,\ x_f = 0.3,\ \alpha = \psi(0, \frac{1}{2}) = -1.1439,\ \lambda^2 = 144.5796.$

See Fig. 2.3 for computations with uncorrected standard scheme.